communications materials

Article

https://doi.org/10.1038/s43246-024-00653-7

Achieving liquid processors by colloidal suspensions for reservoir computing

Check for updates

Raphael Fortulan [1] ✉, Noushin Raeisi Kheirabadi[1], Alessandro Chiolerio [1,2] & Andrew Adamatzky[1]

The increasing use of machine learning, with its significant computational and environmental costs, has motivated the exploration of unconventional computing substrates. Liquid substrates, such as colloids, are of particular interest due to their ability to conform to various shapes while exhibiting complex dynamics resulting from the collective behaviour of the constituent colloidal particles. This study explores the potential of using a PEDOT:PSS colloidal suspension as a physical reservoir for reservoir computing in spoken digit recognition. Reservoir computing uses high-dimensional dynamical systems to perform tasks with different substrates, including physical ones. Here, a physical reservoir is implemented that encodes temporal data by exploiting the rich dynamics inherent in colloidal suspensions, thus avoiding reliance on conventional computing hardware. The reservoir processes audio input encoded as spike sequences, which are then classified using a trained readout layer to identify spoken digits. Evaluation across different speaker scenarios shows that the colloidal reservoir achieves high accuracy in classification tasks, demonstrating its viability as a physical reservoir substrate.

The 20th century saw the emergence of classical computing, given by the computational model formulated by Alan Turing and its physical realisation through the von Neumann architecture (and more recently, the modified Harvard) using semiconductor-based transistors and later integrated circuits. However, unconventional computing offers the exciting prospect of disrupting this long-standing paradigm in the 21st century.

Unconventional computing encompasses a wide range of computing paradigms that push the boundaries of conventional semiconductor-based digital electronics. These paradigms are often inspired by natural phenomena, exploiting the intrinsic computational capabilities of physical, chemical, and/or biological systems. By making use of the unique properties and dynamics of these systems, unconventional computing architectures promise to overcome fundamental limitations of classical computing, such as energy efficiency, fault tolerance, and the ability to directly interface with and process complex analogue signals from the physical world[1].

One of the most widespread and resource-intensive fields today is artificial intelligence and machine learning. Over the last decade, Artificial Neural Networks (ANNs) have become an increasingly dominant technique for information and data processing. ANNs mimic the behaviour of biological systems, with a computational model consisting of neuron-like units connected by weighted links that resemble neural synapses. Recurrent Neural Networks (RNNs) have recently become the most popular type of ANN due to their ability to handle dynamic spatio-temporal data and embed temporal dependencies in their structure, and they are used in major language models such as Google's Gemini and OpenAI's ChatGPT. A striking problem with these models is their enormous computational complexity, which requires not only large amounts of data but also significant energy to power servers and GPUs for their training.

Reservoir computing (RC) is an RNN-based framework that is suitable for processing temporal and sequential information and is derived from echo state networks (ESNs) and liquid state machines (LSMs)[2–8]. The domain of reservoir computing was inspired by Julian Miller's *in materia* computing[9–13].

The paradigm of reservoir computing involves using a highly nonlinear system to map the input signal into a much higher-dimensional space. The state of the reservoir is then harvested using a readout layer and trained to produce the desired output. Not all complex systems are suitable as good reservoirs, as they must exhibit (slowly fading) memory, known as echo state properties, and separability (as shown in Fig. 1). To improve the classification performance of an RC, it is essential to ensure that the reservoir states produced by two different input histories are significantly different (separated).

The reservoir can be either computational, instantiated through numerical models, or physical, harnessing the inherent properties of physical systems. Physical reservoirs offer a significant advantage by circumventing the need for conventional computing architectures and instead leveraging the rich dynamics inherent to various physical substrates to perform high-dimensional mappings and complex transformations.

[1]Unconventional Computing Laboratory, University of the West of England, Coldharbour Ln, Bristol, BS16 1QY, UK. [2]Bioinspired Soft Robotics Laboratory, Istituto Italiano di Tecnologia, Via Morego 30, Genova, 16165, Italy. ✉e-mail: raphael.vicentefortulan@uwe.ac.uk

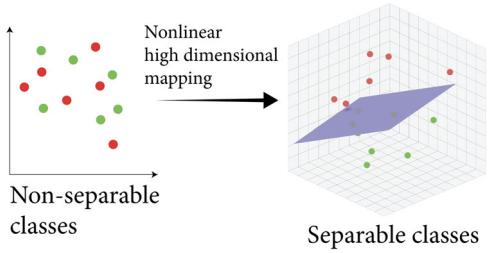

Fig. 1 | Illustration of the separability property of a reservoir due to its nonlinear mapping. The low-dimensional, linearly non-separable feature set are taken to a higher dimension via the reservoir. The new high-dimensional features are now linearly separable via a hyperplane.

Various physical RC implementations have been proposed across different domains, utilising a wide range of physical phenomena. For example, spintronic oscillators, which consist of nanoscale magnetic tunnel junctions, have been shown to function as reservoirs capable of performing tasks such as pattern recognition and time-series prediction[14,15]. In the optical and photonic domains, integrated photonic reservoirs based on delay-coupled systems and coupled semiconductor optical amplifiers show promise for information processing and signal classification[16]. Memristor crossbar arrays, which leverage the voltage-controlled resistance characteristics of these devices, and ferroelectric diodes have also been investigated as physical reservoirs for various machine learning tasks[17,18].

In addition to solid-state implementations, physical RC has also been explored on unconventional substrates, such as field-programmable gate arrays (FPGAs)[19]. Furthermore, liquid systems have been proposed as reservoirs for time-series forecasting and pattern recognition, utilising the chaotic dynamics of turbulent flows. In addition, physical reservoirs made of compliant and deformable materials, known as soft robotic systems, have been shown to encode temporal information in their morphological dynamics[20–22].

Liquid cybernetic systems, conceptualised as colloidal suspensions capable of autonomous information processing, have demonstrated intriguing features, including autolographic capabilities — the ability to self-encode information within their inherent dynamics and morphological reconfigurations[23,24]. Our prior experimental investigations with zinc oxide (ZnO) colloidal suspensions under controlled laboratory conditions have showcased their potential as electrical analogue neuromorphic processors, successfully implementing synaptic plasticity-like learning and emulating Pavlovian conditioning reflexes[25–27]. Complementing these findings, the computational abilities of magnetite (Fe_3O_4) ferrofluid suspensions for handwritten digit recognition have further exemplified the versatility of these liquid-based physical reservoirs for information processing tasks[28].

The autolographic nature of these liquid cybernetic systems can be attributed to the complex dynamics that govern the collective behaviour of the constituent colloidal particles. In the case of ZnO colloids, the self-organised electrohydrodynamic patterns emerging from the interplay between applied electric fields and the electrophoretic mobility of the charged particles enable the encoding and processing of information within the evolving morphologies and spatiotemporal dynamics of the colloidal ensemble[25]. Similarly, for ferrofluids composed of superparamagnetic nanoparticles, the complex magnetohydrodynamic phenomena arising from the coupling between magnetic fields and the fluid flow dynamics facilitate the transduction and processing of information within the reconfigurable patterns exhibited by the colloidal suspension[29].

The advent of colloid-based computing systems represents a significant paradigm shift in computing and materials science, offering a compelling alternative to conventional solid-state systems for operations in harsh environments[23]. These environments, characterised by extreme temperatures, pressures, radiation, or chemical hazards, present significant challenges for traditional computing systems[30]. Colloids, which feature a liquid state of aggregation and are based on highly compliant materials (such as those found in living organisms), offer innovative solutions, particularly in terms of mobility and shape. Colloids also demonstrate minimal resistance to compressive forces, allowing them to conform to different shapes. By integrating the principles of liquid cybernetic systems and the adaptability of colloid-based systems, researchers will be able to develop highly resilient and versatile computing solutions for applications in harsh environments such as deep-sea exploration, post-disaster search and rescue, or interplanetary surface investigations.

In this paper, we investigate the properties of a poly(3,4-ethylenedioxythiophene) polystyrenesulphonate (PEDOT:PSS) colloidal suspension as a physical reservoir for classification of spoken digits. Extensive research has explored the application of PEDOT:PSS in neuromorphic devices due to its advantageous properties, including its potential as a bio-interfacing material and its use in organic electronic devices[31–34]. Its characteristics, such as promising thermoelectric properties, high electrical conductivity, and transparency make it the most widely used conductive polymer[35,36]. PEDOT:PSS exhibits tunable electrical conductivity, high flexibility, and high permeability to gases, making it a promising material to act as a temporary storage or transport path for abundant inflowing ions[37,38].

Here, we show that the combination of history-dependent output and highly nonlinear dynamics aligns with the high complexity present in the interactions of colloidal particles. This creates an ideal scenario for reservoir computing, a paradigm that leverages the inherent dynamics of physical systems for information processing. By utilizing this approach, we were able to effectively perform the classification of utterances from 5 different speakers with distinct accents.

Results and Discussion

Properties of the PEDOT:PSS colloidal suspension

The sequence of partially cationic ethylenedioxythiophene (PEDOT) and anionic styrenesulphonic acid (PSS) monomer units (primary structure, as seen in Fig. 2a) forms a polyion complex of PEDOT oligomers and PSS chains through electrostatic interactions (secondary structure, as seen in Fig. 2b)[39], which is dispersable in water as colloidal gel particles (tertiary structure, as seen in Fig. 2c)[40]. These gel particles display a micelle-like structure in aqueous solutions with a hydrophobic PEDOT-rich core and a hydrophilic PSS-rich shell[41].

The current/voltage characteristics of the colloid were investigated using a scan rate of 0.2 V s^{-1} as seen in Fig. 3a, with the onset potentials for oxidisation and reduction being, respectively, 3.5 V and −3.7 V.

PEDOT changes from its neutral non conductive state to its conductive and oxidised state and decreases the resistance of the liquid[42], following the reaction below

$$\mathrm{PEDOT^{+}{:}\,PSS^{-}} + \mathrm{H^{+}} + \mathrm{e^{-}} \rightleftharpoons \mathrm{PEDOT^{0}} + \mathrm{H^{+}{:}\,PSS^{-}}. \quad (1)$$

This charge and discharge phenomenon that induces changes in the resistance of the materials is related to the doping and de-doping that occur in intrinsically conductive polymers[43] and results in the flow of positive or negative ions along the polymer chain.

The $I-V$ curve shown in Fig. 3a exhibits the typical pinched hysteresis loop of a classical memristor[44]. The current/voltage characteristics of the materials show both a history-dependent output and highly nonlinear dynamics[45–51], both essential to RC.

Colloidal particles typically interact through nonspecific forces such as van der Waals attraction and electrostatic repulsion, naturally progressing towards an equilibrium state. However, when an external field is applied, the energy landscape of these polarisable particles is altered, driving them away from equilibrium and onto alternative pathways that would otherwise be inaccessible. This process leads to the formation of suprastructures influenced by the external field[52–54].

At this scale, the fluid dynamics of the particles are characterised by a low Reynolds number, $\mathrm{Re} = \frac{\rho v L}{\mu}$, where ρ and μ denote, respectively, the density and viscosity of the fluid, and v and L represent, respectively, the velocity and characteristic length of the object. This parameter, which

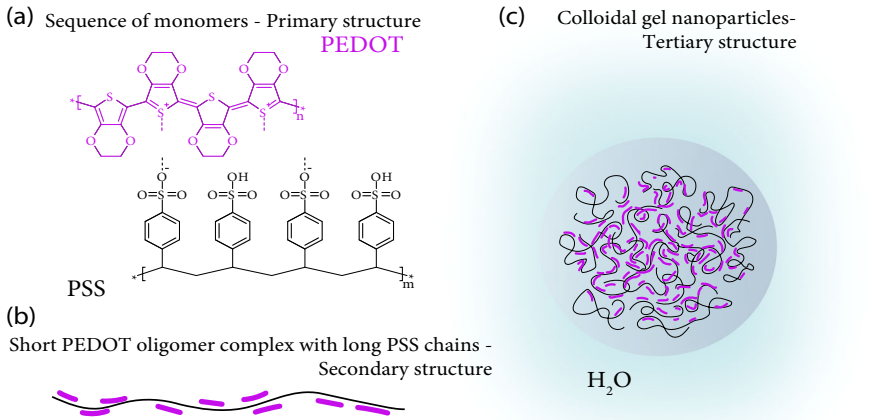

Fig. 2 | PEDOT:PSS structure. a Chemical structure of PEDOT:PSS. **b** Cationic oligomeric PEDOT attached to a long anionic PSS chain. **c** Dispersed colloidal gel nanoparticle in water.

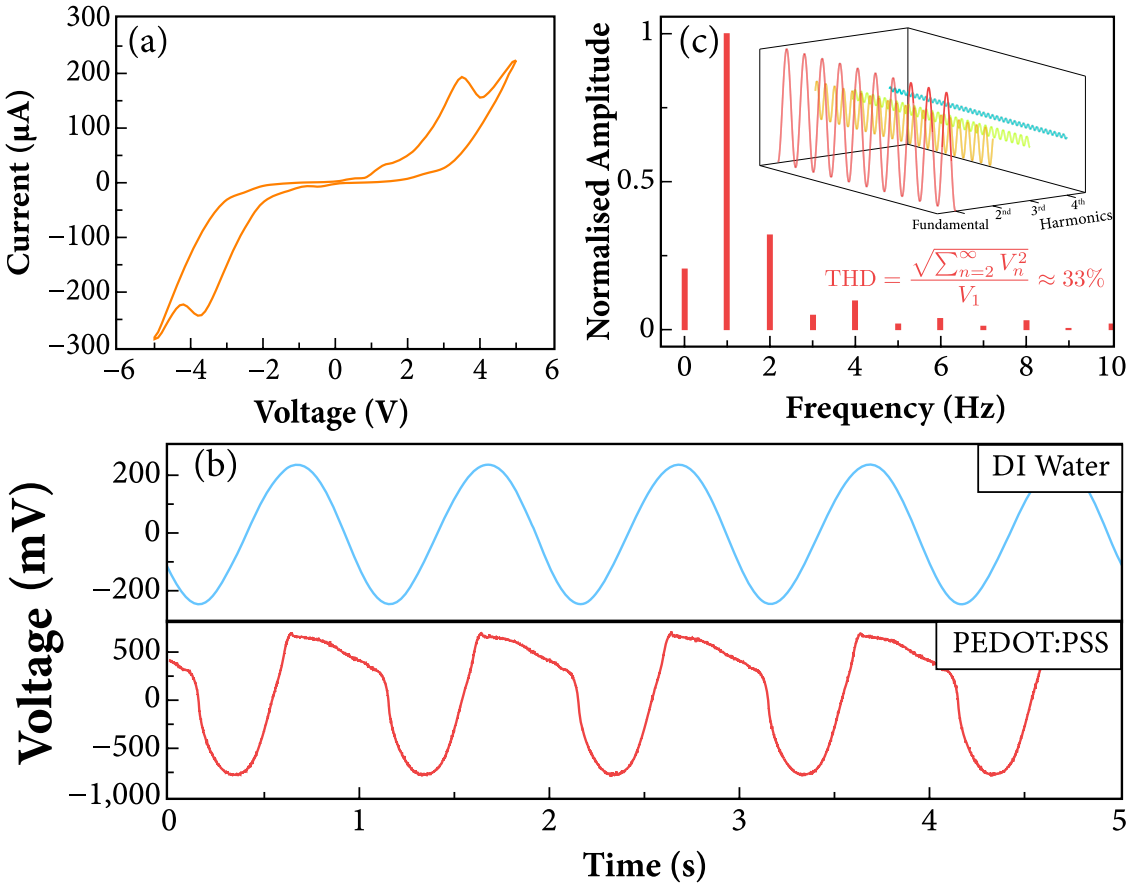

Fig. 3 | Electrical properties of the PEDOT:PSS colloid. a $I-V$ curve from −5 V to 5 V for the PEDOT:PSS colloid. **b** Measured output voltage induced by an input sine wave for both the PEDOT:PSS colloid and deionised (DI) water. **c** Fourier transform of the recorded measured output voltage of the PEDOT:PSS colloid. The formula displayed in the plot shows the calculated total harmonic distortion (THD) of the signal, and the inset displays both the fundamental component and the second, third, and fourth harmonics.

correlates with the viscous behaviour of all Newtonian fluids, is the ratio of inertial forces (resistant to change or motion) to viscous forces (dominated by fluid viscosity) acting on a particle immersed in the fluid[55].

Colloids, having characteristic lengths on the order of micrometres, exhibit Reynolds numbers in water that are significantly lower than 1 ($Re \ll 1$). This indicates a regime of creeping motion where inertial forces are negligible compared to viscous forces[55]. For colloids solvated in water, the fluid behaves as viscous as molasses does to humans. A key consequence of such low Reynolds numbers is articulated by the scallop theorem[56], which states that no momentum can be accumulated while swimming through the fluid. Therefore, the dissipation of the resulting structures is not instantaneous, emphasising the memory effect of the colloidal arrangements (see Fig. S2 in Supplementary Information for an illustration of the presence of memory in the colloidal suspension).

The necessity of highly nonlinear dimensional mapping in reservoirs is largely fulfilled by the motion of particles within the fluid. Colloids behave

similarly to large atoms due to their Brownian motion[57], which is inherent to small particles and their susceptibility to thermal noise. Consequently, colloidal motion is inherently random and complex[58].

Furthermore, introducing stimuli such as electric fields, direct electric currents, and induced magnetic fields within the colloidal suspension, creates a number of side effects that perturb the dynamics of particle movements, including the Ludwig-Soret effect, magnetic advection, electro-osmosis, and dielectrophoretic effects, making the system a very complex and chaotic substrate[59]. Figure 3b and S1 (in Supplementary Information) show that the nonlinear behaviour is mediated by the ion drift in suspension, which responds to the time-varying local electric field to change the ionic states of the reservoir. The Fourier transform of the measured voltage in the colloidal suspension, shown in Fig. 3c, demonstrates the high degree of nonlinearity of the suspension, with the presence of a high harmonic distortion (as illustrated by the inset)[60].

Theoretical background of reservoir computing

Let $\mathbf{u}(t) \in \mathbb{R}^M$ be the M continuous-in-time input signals and $\mathbf{u}_j = [u_{1,j}, u_{2,j}, \ldots, u_{M,j}]^\intercal, j = 0, 1, \ldots, T-1$, where T is the number of points in the training dataset, be the discrete time version of $u(t)$ at a time t_j.

The input signals are projected into the high-dimensional reservoir composed of N interconnected nodes by a matrix $\mathbf{W}_{\text{in}} \in \mathbb{R}^{N \times M}$. The reservoir is represented by an adjacency matrix $\mathbf{W} \in \mathbb{R}^{N \times N}$ and encodes the strength of each pair of nodes. In our case of a physical reservoir, both $\mathbf{W}_{\text{in}}$ and $\mathbf{W}$ are determined by our experimental system and colloidal suspension.

The difference equation representing the reservoir is then

$$\mathbf{x}_{j+1} = (1-\alpha)\mathbf{x}_j + \alpha f(\mathbf{W}\mathbf{x}_j + \mathbf{W}_{\text{in}}\mathbf{u}_j + \mathbf{b}), \tag{2}$$

where α is the leaking rate, $\mathbf{x}_j \in \mathbb{R}^N$ is the state vector at a time t_j, f is the activation function, and $\mathbf{b}$ is the bias vector. For the classification problem, here, we extended the state vector in time by defining

$$\mathbf{a} = [\mathbf{x}_0^\intercal, \mathbf{x}_1^\intercal, \ldots, \mathbf{x}_{T-1}^\intercal]^\intercal. \tag{3}$$

where $\mathbf{a}$ is the extended state vector in time.

The output layer of the reservoir is a linear transformation of the accumulation vector $\mathbf{a}$, $\mathbf{W}_{out} \in \mathbb{R}^{C \times N \times T}$

$$\mathbf{o} = \mathbf{W}_{\text{out}}\mathbf{a}, \tag{4}$$

where C is the number of classes.

Finally, the normalised probabilities vector $\hat{\mathbf{y}}$ is given by

$$\hat{\mathbf{y}} = \text{softmax}(\mathbf{o}), \tag{5}$$

where

$$\hat{y}_k = \text{softmax}(o_k) = \frac{\exp(o_k)}{\sum_l \exp(o_l)} \tag{6}$$

maps a vector of real numbers into a vector of probabilities. Each probability $\hat{y}_k \in [0, 1]$ and the sum of the probabilities is 1. The output layer is trained using supervised training with a cross-entropy loss function

$$L = -\sum_{k=1}^{C} y_k \log \hat{\mathbf{y}}_k, \tag{7}$$

where $y_k \in \{0, 1\}$ indicates whether the class label k was correctly ($y_k = 1$) or incorrectly ($y_k = 0$) classified.

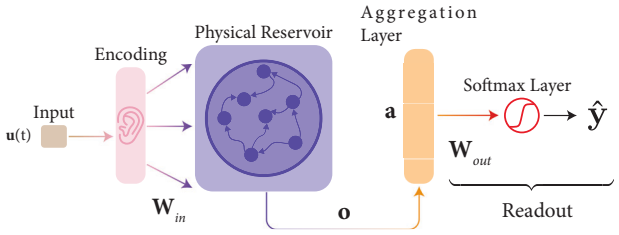

Fig. 4 | Architecture of the physical reservoir based classifier. The diagram shows how the data is first encoded, processed at the physical reservoir, the output of the reservoir is aggregated, and then passed through a trainable readout layer to generate a set of probabilities for classification.

Table 1 | Classification performance for the reservoir based classifier in a speaker-dependent scenario

Speaker	Accuracy (%)
1	84.04
2	85.25
3	84.65
4	80
5	75.15
6	83.84
Avg.	82.15
Std.	3.89

Here, to avoid overfitting, we also added a L1-regularisation term in the loss function; thus, the final loss function can be written as

$$L = -\sum_{k=1}^{C} y_k \log \hat{\mathbf{y}}_k + \lambda \sum_{1}^{C} |w_{k,out}|, \tag{8}$$

where λ is the regularisation factor and $w_{k,out}$ is the k-th column of $\mathbf{W}_{out}$.

The final architecture used in this work is shown in Fig. 4.

Speaker-dependent scenario

In the speaker-dependent scenario, each speaker was evaluated separately, and the accuracy of the classifier was evaluated individually. In Table 1, the accuracy obtained for the reservoir trained with each individual speaker is shown. Our reservoir framework has proven to be able to correctly classify the spoken digits with large accuracy, even though the dataset is small. The minimum value of accuracy was of 75.15%, the maximum was 85.25%, and the average value between all speakers was of 82.15%.

To understand how the classifier was performing in the classification of each digit, in Fig. 5, the average confusion matrix of all experiments is shown. The matrix is almost perfectly diagonal, which indicates that the reservoir was able to successfully classify all digits in a similar manner.

The high separability capabilities of our physical reservoir, which enabled a classification accuracy of over 80%, are illustrated in Fig. 6, where the utterances, their corresponding spike representations, and the measured electrical signals from the reservoir are shown for the spoken digits “0”, ”5”, and “9” from the same speaker. In particular, the measured responses shown in Fig. 6g–i exhibit highly nonlinear behaviour and strikingly different visual characteristics across the different spoken digits.

Speaker-independent scenario. In this speaker-independent scenario, the reservoir was trained on utterances from one speaker and tested on the data from the remaining speakers. As no data from other speakers was included in the training, this experiment tested the fundamental ability of our physical reservoir computing architecture to adapt to and learn from

a very small sample of data. The aim was to determine whether it was possible for the reservoir to infer the correct digit labels from such limited training examples for a single speaker.

The results for each individual speaker in this single-speaker training setting are shown in Table 2, which shows the accuracy obtained for the reservoir trained on each speaker's data. As expected, the classification accuracy was quite poor across all speakers, with an average of only 7.91% and a maximum of only 9.49%. This poor performance is a direct result of the extremely small amount of training data provided to the reservoir in this state. With so few examples, not enough variability in the spoken digits was presented for the reservoir to effectively learn separable representations and generalise digit classification to novel examples from that speaker.

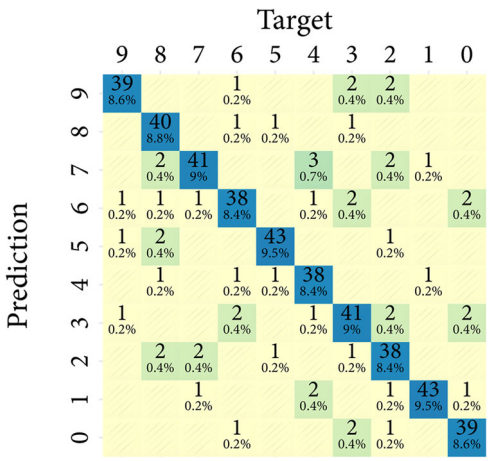

Fig. 5 | Average confusion matrix for the speaker-dependent scenario. Average confusion matrix for the speaker-dependent scenario, where training and testing were performed for each speaker. Averaged counts and normalised percentages are displayed for each digit.

Furthermore, the presence of data from only a single speaker during training may have led to an overfitting of the classifier dynamics in the reservoir system. Rather than learning general representations of digit classes that are invariant to speaker features, it is likely that the reservoir preferentially encoded speaker-specific features and features that were specific to that individual's vocal patterns, and this could explain why performance was so low for all speakers as the classifier failed to extract robust, general features of each digit class.

The average confusion matrix across all single speaker experiments, shown in Fig. 7, illustrates the poor classification performance. There is a high degree of false negatives for each digit label, indicating that the reservoir was unable to reliably separate any of the digit classes under this extremely data-limited single-speaker training regime.

These results are not surprising given the inherent complexity of the spoken digit classification task and the fact that the reservoir was only exposed to a handful of training examples from a single speaker. In the next scenarios, we will show that it is possible for the classifier to improve rapidly.

In this speaker-independent scenario, the reservoir was trained using two speakers' utterances and tested on the remaining data from the dataset. Since the order in which the data is being applied to the reservoir is considered indifferent, a total of 15 combinations of the two speakers were considered for training and testing.

The results for each of these 15 combinations are shown in Table 3, which presents the accuracy obtained for the reservoir trained with each individual combination of the two speakers. The performance of the classifier was greatly improved when trained on data from two speakers, if compared with the training using just one speaker's data. Specifically, there was a fourfold increase in the average accuracy across the 15 combinations

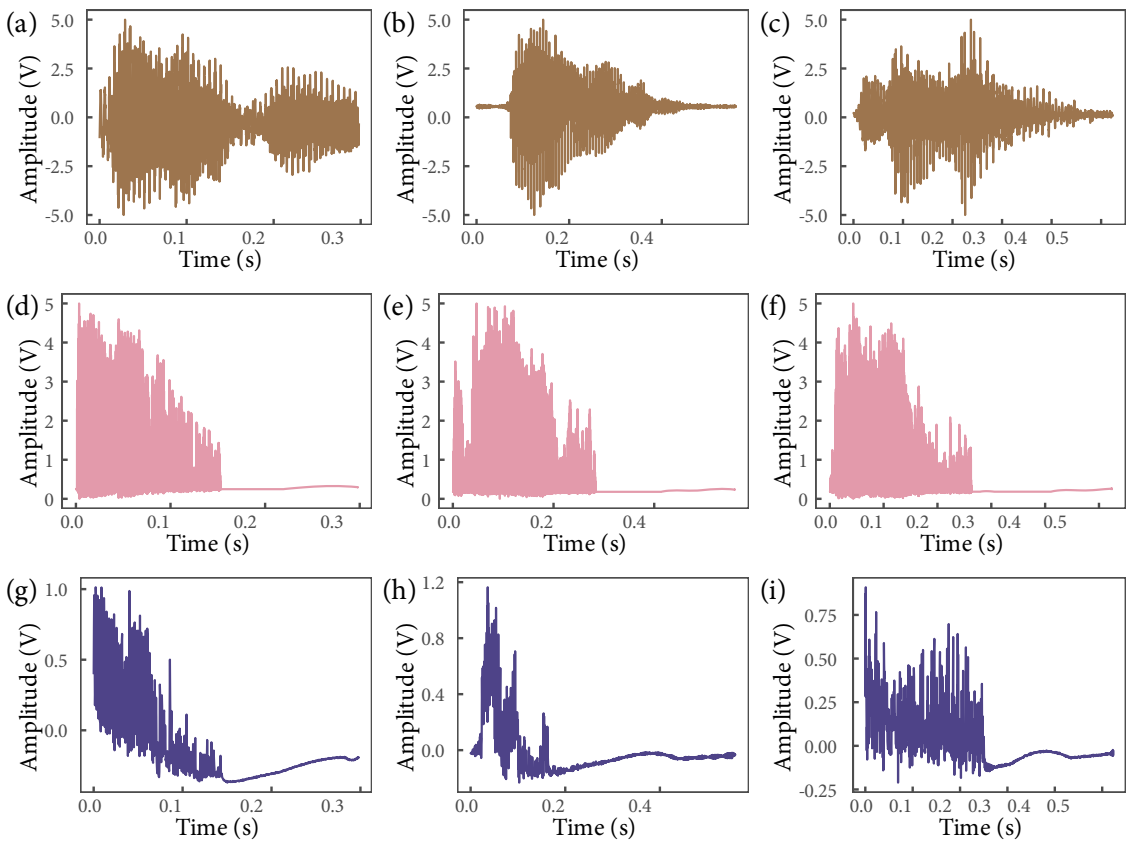

Fig. 6 | Example of utterances, spike representation, and measured signals for the reservoir. a–c Utterances for "0", "5", "9", respectively. **d–f** Spike representations for "0", "5", and "9", respectively. **g–i** Measured signals for "0", "5", and "9", respectively.

Table 2 | Classification performance of the reservoir-based classifier in a speaker-independent scenario, trained on one speaker and tested on the remaining data

Speaker used in training	Accuracy (%)
1	5.64
2	8.76
3	7.70
4	8.26
5	7.65
6	9.49
Avg.	7.91
Std.	1.31

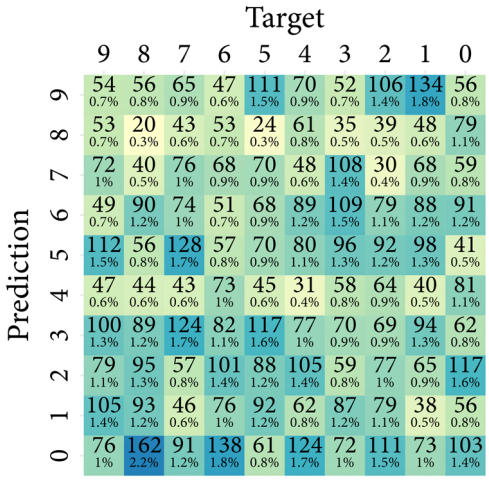

Fig. 7 | Average confusion matrix for speaker-independent scenario trained with a single speake. Average confusion matrix for the speaker-independent scenario, where a single speaker was used for training and testing on the remaining data. Averaged counts and normalised percentages are displayed for each digit.

compared to the single speaker case. This result demonstrates that our physical reservoir architecture benefited substantially from the larger dataset created by combining data from multiple speakers. Remarkably, it was able to generalise well for digit classification even with this relatively small increase in the number of training samples and variety of speakers.

This improved generalisation ability is further illustrated in Fig. 8 where the average confusion matrix across all 15 experimental combinations is displayed. Compared to the confusion matrix for the single speaker case shown previously in Fig. 5, it can be clearly seen that the degree of false negative errors for each digit class is greatly reduced when training on the combined two-speaker data. However, some digits remained more challenging to classify correctly than others. Notably, the digit 0 was the one that displayed the largest number of misclassification errors across the 15 two-speaker combinations on average.

Full dataset

In this scenario, where the reservoir was trained on data from all speakers in the dataset, the classification accuracy reached 56.83%. Although not outstanding, this level of performance suggests that our physical reservoir computing approach has a significant ability to learn generalised representations and effectively classify spoken digit signals from multiple speakers with some degree of accuracy, even when trained on limited data.

The difficulty of achieving high recognition accuracy from small sample sizes is a significant challenge not only for traditional gradient-based machine learning techniques but for any pattern recognition system tasked with learning from sparse data. However, the reservoir demonstrated its

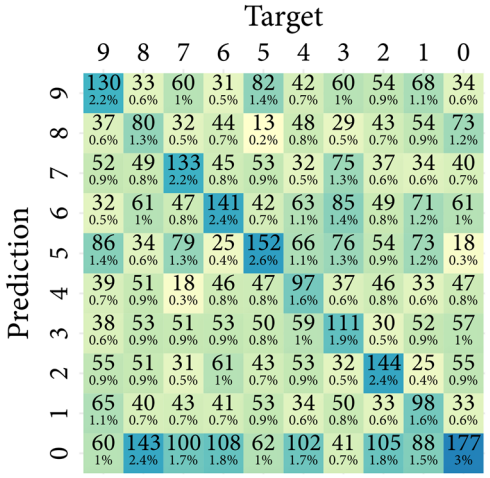

Fig. 8 | Average confusion matrix for speaker-independent scenario trained with two speaker. Average confusion matrix for the speaker-independent scenario, where the reservoir was trained on two speakers and tested on the remaining ones. Averaged counts and normalised percentages are shown for each digit.

potential value by achieving 56.83% accuracy on this multi-speaker task after training on the dataset in a single, efficient computation phase.

This competitive performance, achieved by effectively just training the output layer, exemplifies two key practical advantages of reservoir computation over conventional gradient-descent methods: minimal training time requirements and the ability to rapidly encode general signal features from limited data into high-dimensional transient dynamics. These attributes make reservoir approaches particularly suitable for applications where training data is costly or time-consuming to acquire, or where rapid model adaptation is essential.

Analysis of the confusion matrix for the multi-speaker scenario, shown in Fig. 9, shows that although overall accuracy was modest, the classifier was able to correctly identify examples from all digit classes to some extent when trained on the combined speaker data.

Conclusions

In this paper, we present a colloidal suspension of PEDOT:PSS as a physical reservoir for spoken-digit recognition tasks using reservoir computing.

In a speaker-dependent scenario, we achieved an average accuracy of 82.15% when tested on individual speakers, demonstrating the reservoir's ability to effectively separate and classify different spoken digits. For the speaker-independent scenario, with limited training data from one or two speakers, the system's performance improved significantly when trained on data from multiple speakers, achieving up to 46.45% average accuracy. When trained on the full dataset with all speakers, we achieved a reasonable accuracy of 56.83% for the multi-speaker spoken digit recognition task, despite the use of limited data. Our study highlights the potential of using unconventional computational substrates such as colloidal suspensions, which can exploit their inherent nonlinear dynamics and high-dimensional encoding capabilities to perform machine learning tasks without direct training of the physical system. This work contributes to the emerging field of colloid-based computing systems. The use of PEDOT:PSS in a colloidal form combines the advantages of liquid cybernetic systems with the unique properties of this conductive polymer, paving the way for highly resilient and versatile computing solutions.

Methods

PEDOT:PSS suspension synthesis

Analytical grade PEDOT:PSS suspension (3.0–4.0% in H_2O, high conductivity grade) was obtained from Merck. 200 μl of PEDOT:PSS was subjected to ultrasonication for 0.5 h. The aqueous PEDOT:PSS was then placed in a plastic Petri dish for further experiments.

Table 3 | Classification performance of the reservoir-based classifier in a speaker-independent scenario, using a training set of two speakers and testing on the remaining data

Set of speakers used in training	Accuracy (%)
[1,2]	32.30
[1,3]	32.40
[1,4]	38.13
[1,5]	46.45
[1,6]	35.05
[2,3]	6.87
[2,4]	23.42
[2,5]	26.20
[2,6]	32.40
[3,4]	24.63
[3,5]	30.43
[3,6]	38.13
[4,5]	30.35
[4,6]	46.45
[5,6]	33.57
Avg.	31.79
Std.	9.85

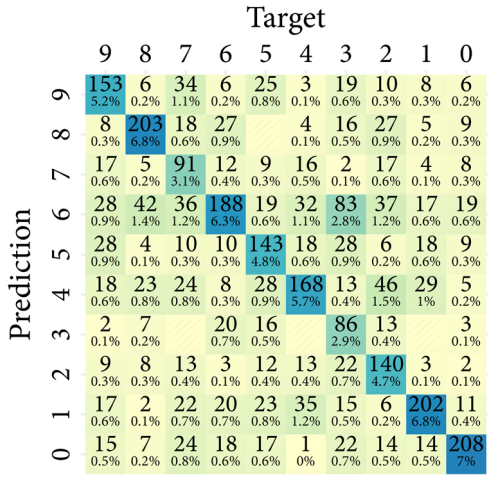

Fig. 9 | Confusion matrix for full dataset. Confusion matrix for speaker classification in the case where the reservoir was trained with data from all speakers.

PEDOT:PSS characterisation

Current/voltage characterisation was conducted with the help of a Keithley 2450 sourcemeter. A PC-based oscilloscope (PicoTechnology, PicoScope 5442D) was used to generate and measure the sine wave signals in the colloid and deionised water. All electrical measurements were carried out using Pt/Ir probes at room temperature in air.

Experimental setup and datasets for reservoir computing

The Free Spoken Digit Dataset (FSDD)[61] was selected to evaluate the proposed framework. It is a free, open-source speech dataset that includes recordings of spoken digits from 0 to 9, each approximately 0.5 s long, in 16-bit 8 kHz mono .WAV files. The dataset consists of 3000 utterances in English from six speakers (50 repetitions of each digit per speaker) with different accents. To explore the neuromorphic response of the reservoir, the FSDD dataset was encoded into a spike sequence that represents the human auditory-nerve transformation of acoustic signals, following the method described by Zilany et al.[62,63]. This encoding was performed using the Auditory Modelling Toolbox (AMT) version 1.5[64] in Octave 8.4.0. This approach allows us to assess the capacity of the reservoir to classify auditory information in a format similar to that processed by the human auditory system, following the premise of neuromorphic computing[65,66], while also providing a simplified signal representation that may enhance the reservoir's classification accuracy.

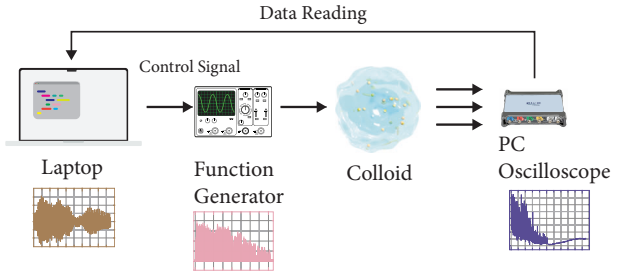

Fig. 10 | Experimental setup for the physical reservoir. A laptop is used to process the audio data and send the control signal to a function generator. The function generator produces a voltage signal, which is applied to the colloid. The electrical response is measured on three channels by a PC based oscilloscope and sent back to the laptop for processing. The plots show the audio signal, its spike representation, and the measured electrical response of the colloid.

Training and testing were evaluated using three different schemes. First, we evaluated a speaker-dependent scenario, where the classifier was trained and tested using only the utterances of one individual speaker. A 66%/33% split in stratified fashion was used for training and testing, and the split was made in a stratified fashion to maintain balance between the classes. Subsequently, we proceeded with a *k*-fold cross-validation on speaker-independent scenarios, where the classifier was trained and tested using one/two speaker(s) and tested on the remaining. The final accuracy was the average value between all possible combinations. Finally, a 66%/33% stratified split for training and testing was used for the whole dataset. All features were normalised before training, and the training time for the readout layer in all experiments was less than 650 ms.

Besides encoding, the results for this paper were evaluated using Python 3.11.5 on an ARM-based CPU running macOS. The output layer was trained using TensorFlow 2.12.0[67].

The spike signals were applied to the colloidal suspension using an arbitrary function generator (RIGOL, DG4162), controlled via Ethernet using the LXI protocol implemented with the python-vxi11 module on a laptop, and a 10 μm Pt/Ir probe. The signals were normalised so that the highest peak corresponded to 5 V. Three output Pt/Ir probes, spaced 5 mm apart, were positioned 5 mm from the input probe and connected to a PC-based oscilloscope (Pico Technology, PicoScope 5442D). The measured voltage was sent to the same laptop for data processing. The experimental setup for the physical reservoir is shown in Fig. 10.

Data availability

Datasets generated during the current study are available from 10.5281/zenodo.13786593. The Free Spoken Digit Dataset (FSDD) is available at https://github.com/Jakobovski/free-spoken-digit-dataset.

Received: 29 March 2024; Accepted: 23 September 2024;
Published online: 28 September 2024

References

1. Adamatzky, A. *Handbook of Unconventional Computing: Volume 2: Implementations*, vol. 2 (World Scientific, 2021).
2. Verstraeten, D., Schrauwen, B., d'Haene, M. & Stroobandt, D. An experimental unification of reservoir computing methods. *Neural Netw.* **20**, 391–403 (2007).

3. Obst, O. & Boedecker, J. Guided self-organization of input-driven recurrent neural networks. In *Guided self-organization: Inception*, 319–340 (Springer, 2014).
4. Dale, M., Miller, J. F. & Stepney, S. Reservoir computing as a model for in-materio computing. *Advances in Unconventional Computing: Volume 1: Theory* 533–571 (2017).
5. Konkoli, Z., Nichele, S., Dale, M. & Stepney, S. Reservoir computing with computational matter. In *Computational Matter*, 269–293 (Springer, 2018).
6. Athanasiou, V. & Konkoli, Z. On using reservoir computing for sensing applications: exploring environment-sensitive memristor networks. *Int J. Parallel, Emergent Distrib. Syst.* **33**, 367–386 (2018).
7. Konkoli, Z. On developing theory of reservoir computing for sensing applications: the state weaving environment echo tracker (sweet) algorithm. *Int J. Parallel, Emergent Distrib. Syst.* **33**, 121–143 (2018).
8. Dale, M., Miller, J. F., Stepney, S. & Trefzer, M. A. A substrate-independent framework to characterize reservoir computers. *Proc. R. Soc. A* **475**, 20180723 (2019).
9. Miller, J. F. & Downing, K. Evolution in materio: Looking beyond the silicon box. In *Proceedings 2002 NASA/DoD Conference on Evolvable Hardware*, 167–176 (Ieee, 2002).
10. Miller, J. F., Harding, S. L. & Tufte, G. Evolution-in-materio: evolving computation in materials. *Evol. Intell.* **7**, 49–67 (2014).
11. Stepney, S. Co-designing the computational model and the computing substrate. In *Unconventional Computation and Natural Computation: 18th International Conference, UCNC 2019, Tokyo, Japan, June 3–7, 2019, Proceedings 18*, 5–14 (Springer, 2019).
12. Miller, J. F., Hickinbotham, S. J. & Amos, M. In materio computation using carbon nanotubes. In *Computational Matter*, 33–43 (Springer, 2018).
13. Miller, J. F. The alchemy of computation: designing with the unknown. *Nat. Comput* **18**, 515–526 (2019).
14. Tsunegi, S. et al. Physical reservoir computing based on spin torque oscillator with forced synchronization. *Appl Phys. Lett.* **114**, 164101 (2019).
15. Torrejon, J. et al. Neuromorphic computing with nanoscale spintronic oscillators. *Nature* **547**, 428–431 (2017).
16. Takano, K. et al. Compact reservoir computing with a photonic integrated circuit. *Opt. Express* **26**, 29424–29439 (2018).
17. Milano, G. et al. In materia reservoir computing with a fully memristive architecture based on self-organizing nanowire networks. *Nat. Mater.* **21**, 195–202 (2022).
18. Chen, Z. et al. All-ferroelectric implementation of reservoir computing. *Nat. Commun.* **14**, 3585 (2023).
19. Alomar, M. L. et al. Digital Implementation of a Single Dynamical Node Reservoir Computer. *IEEE Trans. Circuits Syst. II: Express Briefs* **62**, 977–981 (2015).
20. Hauser, H., Nanayakkara, T. & Forni, F. Leveraging morphological computation for controlling soft robots: Learning from nature to control soft robots. *IEEE Control Syst. Mag.* **43**, 114–129 (2023).
21. Bhovad, P. & Li, S. Physical reservoir computing with origami and its application to robotic crawling. *Sci. Rep.* **11**, 13002 (2021).
22. Polygerinos, P. et al. Soft robotics: Review of fluid-driven intrinsically soft devices; manufacturing, sensing, control, and applications in human-robot interaction. *Adv. Eng. Mater.* **19**, 1700016 (2017).
23. Chiolerio, A. & Quadrelli, M. B. Smart fluid systems: The advent of autonomous liquid robotics. *Adv. Sci.* **4**, 1700036 (2017).
24. Chiolerio, A. Liquid cybernetic systems: the fourth-order cybernetics. *Adv. Intell. Syst.* **2**, 2000120 (2020).
25. Kheirabadi, N. R., Chiolerio, A., Phillips, N. & Adamatzky, A. Learning in colloids: Synapse-like zno+ dmso colloid. *Neurocomputing* **557**, 126710 (2023).
26. Raeisi Kheirabadi, N., Chiolerio, A. & Adamatzky, A. Pavlovian reflex in colloids. *BioNanoSci.* 1–9 (2024).
27. Roberts, N. et al. Logicalcircuits in colloids. *R. Soc. Open Sci.* **11**, 231939 (2024).
28. Crepaldi, M. et al. Experimental demonstration of in-memory computing in a ferrofluid system. *Adv. Mater.* **35**, 2211406 (2023).
29. Cecchini, L. & Chiolerio, A. The magnetic body force in ferrofluids. *J. Phys. D: Appl. Phys.* **54**, 355002 (2021).
30. Kalita, H. & Thangavelautham, J. Exploration of Extreme Environments with Current and Emerging Robot Systems. *Curr. Robot Rep.* **1**, 97–104 (2020).
31. Romeo, A. et al. A bio-inspired memory device based on interfacing physarum polycephalum with an organic semiconductor. *APL materials***3** (2015).
32. Tarabella, G. et al. A hybrid living/organic electrochemical transistor based on the physarum polycephalum cell endowed with both sensing and memristive properties. *Chem. Sci.* **6**, 2859–2868 (2015).
33. Tarabella, G. et al. Organic electrochemical transistors monitoring micelle formation. *Chem. Sci.* **3**, 3432–3435 (2012).
34. Luo, X., Ming, J., Gao, J., Ling, H. & Xie, L. Low-power flexible organic memristor based on pedot: Pss/pentacene heterojunction for artificial synapse. *Front Neurosci.* **16**, 1016026 (2022).
35. Lee, J. H. et al. Highly conductive, stretchable, and transparent pedot: Pss electrodes fabricated with triblock copolymer additives and acid treatment. *ACS Appl Mater. interfaces* **10**, 28027–28035 (2018).
36. Wang, Y. et al. Flexible *n* -Type Abundant Chalcopyrite/PEDOT:PSS/Graphene Hybrid Film for Thermoelectric Device Utilizing Low-Grade Heat. *ACS Appl Mater. Interfaces* **13**, 51245–51254 (2021).
37. Feng, Y. et al. Solution-processed polymer thin-film memristors with an electrochromic feature and frequency-dependent synaptic plasticity. *Adv. Intell. Syst.* **1**, 1900022 (2019).
38. John, R. A. et al. Diffusive and drift halide perovskite memristive barristors as nociceptive and synaptic emulators for neuromorphic computing. *Adv. Mater.* **33**, 2007851 (2021).
39. Takano, T., Masunaga, H., Fujiwara, A., Okuzaki, H. & Sasaki, T. PEDOT Nanocrystal in Highly Conductive PEDOT:PSS Polymer Films. *Macromolecules* **45**, 3859–3865 (2012).
40. Horii, T., Li, Y., Mori, Y. & Okuzaki, H. Correlation between the hierarchical structure and electrical conductivity of PEDOT/PSS. *Polym. J.* **47**, 695–699 (2015).
41. Kim, N. et al. Highly Conductive PEDOT:PSS Nanofibrils Induced by Solution-Processed Crystallization. *Adv. Mater.* **26**, 2268–2272 (2014).
42. Marzocchi, M. et al. Physical and Electrochemical Properties of PEDOT:PSS as a Tool for Controlling Cell Growth. *ACS Appl Mater. Interfaces* **7**, 17993–18003 (2015).
43. Eun, J., Kim, D. & Kim, F. S. Electrochemical Doping and Dedoping Behaviors of PEDOT-Based Ternary Conducting Polymer Composites with Binary Polymer Surfactants. *ACS Appl Polym. Mater.* **5**, 5495–5502 (2023).
44. Chua, L. O. & Kang, S. M. Memristive devices and systems. *Proc. IEEE* **64**, 209–223 (1976).
45. Cao, J. et al. Emerging dynamic memristors for neuromorphic reservoir computing. *Nanoscale* **14**, 289–298 (2022).
46. Zhong, Y. et al. Dynamic memristor-based reservoir computing for high-efficiency temporal signal processing. *Nat. Commun.* **12**, 408 (2021).
47. Du, C. et al. Reservoir computing using dynamic memristors for temporal information processing. *Nat. Commun.* **8**, 2204 (2017).
48. Gawai, U., Wu, C.-H., Kumar, D. & Chang, K.-M. Interface Ion-Driven, Highly Stable Synaptic Memristor for Neuromorphic Applications. *ACS Appl Electron Mater.* **5**, 2439–2446 (2023).
49. Wang, P. et al. Ferroelectric Nitride Heterostructures on CMOS Compatible Molybdenum for Synaptic Memristors. *ACS Appl Mater. Interfaces* **15**, 18022–18031 (2023).
50. Rahmani, M. K. et al. Memristive and synaptic characteristics of nitride-based heterostructures on si substrate. *Nanomaterials* **10**, 994 (2020).
51. Zhong, G. et al. Flexible electronic synapse enabled by ferroelectric field effect transistor for robust neuromorphic computing. *Applied Physics Letters* **117** (2020).

52. Ferrar, J. A. & Solomon, M. J. Kinetics of colloidal deposition, assembly, and crystallization in steady electric fields. *Soft matter* **11**, 3599–3611 (2015).
53. Zhang, J., Yang, J., Zhang, Y. & Bevan, M. A. Controlling colloidal crystals via morphing energy landscapes and reinforcement learning. *Sci. Adv.* **6**, eabd6716 (2020).
54. Sullivan, M. T. et al. An electric bottle for colloids. *Phys. Rev. Lett.* **96**, 015703 (2006).
55. White, F. M., Ng, C. O. & Saimek, S.*Fluid Mechanics* (McGraw-Hill, cop., 2011).
56. Purcell, E. M. Life at low Reynolds number. *Am. J. Phys.* **45**, 3–11 (1977).
57. Poon, W. Colloids as Big Atoms. *Science* **304**, 830–831 (2004).
58. Israelachvili, J. N.*Intermolecular and Surface Forces* (Elsevier Science, 2011).
59. Bevione, M., Cecchini, L., Garofalo, E., Suslov, S. A. & Chiolerio, A. Colloidal Technologies for Heat Energy Recovery. In *Heat Energy Recovery for Industrial Processes and Waste*, 49–104 (Springer International Publishing, Cham, 2023).
60. Ieee. IEEE Standard for Harmonic Control in Electric Power Systems. *IEEE Std 519-2022 (Revision of IEEE Std 519-2014)* 1–31 (2022).
61. Jackson, Z. et al. Free spoken digit dataset (FSDD) v1.0.10. https://github.com/Jakobovski/free-spoken-digit-dataset [Accessed 04-03-2024] (2020).
62. Zilany, M. S. A., Bruce, I. C. & Carney, L. H. Updated parameters and expanded simulation options for a model of the auditory periphery. *J. Acoustical Soc. Am.* **135**, 283–286 (2014).
63. Zilany, M. S. A., Bruce, I. C., Nelson, P. C. & Carney, L. H. A phenomenological model of the synapse between the inner hair cell and auditory nerve: Long-term adaptation with power-law dynamics. *J. Acoustical Soc. Am.* **126**, 2390–2412 (2009).
64. Majdak, P., Hollomey, C. & Baumgartner, R. AMT 1.x: A toolbox for reproducible research in auditory modeling. *Acta Acust.* **6**, 19 (2022).
65. Xu, M. et al. Reconfigurable Neuromorphic Computing: Materials, Devices, and Integration. *Adv. Mater.* **35**, 2301063 (2023).
66. Prakash, C. et al. Computing of neuromorphic materials: An emerging approach for bioengineering solutions. *Mater. Adv.* **4**, 5882–5919 (2023).
67. Abadi, M. et al. {TensorFlow}: A system for {Large-Scale} machine learning. In *12th USENIX Symposium on Operating Systems Design and Implementation (OSDI 16)*, 265–283 (2016).

Acknowledgements

R.F., N.R.H., A.C., and A.A. received support from the European Innovation Council and SMEs Executive Agency (EISMEA) under grant agreement No. 964388.

Author contributions

A.C. conceived the concept of computing with colloids. A.A. conceived the concept of sound recognition via patterns of electrical activity. R.F. and N.R.K. carried out the experiments. R.F. performed the data analysis. R.F., N.R.K., A.C., and A.A. contributed to the interpretation of the results. R.F. took the lead in writing the manuscript. A.C. and A.A. were responsible for project supervision and funding acquisition. All authors provided critical feedback and helped shape the research, analysis, and manuscript.

Competing interests

The authors declare no competing interests.

Additional information

Supplementary information The online version contains supplementary material available at https://doi.org/10.1038/s43246-024-00653-7.

Correspondence and requests for materials should be addressed to Raphael Fortulan.

Peer review information *Communications materials* thanks the anonymous reviewers for their contribution to the peer review of this work. Primary Handling Editors: Reinhard Maurer and Aldo Isidori.